Optical Fiber for Distributed Sensing in Harsh Environments

Jie Li[1*], Xiaoguang Sun, Lei Huang, and Andrei Stolov

OFS, 55 Darling Drive, Avon, CT, 06001, USA

ABSTRACT

Optical fibers for telecommunications are designed to transmit light in a relatively benign and protected environment. The design aims to ensure minimal levels of attenuation, optical non-linearity, and other detrimental effects caused by external perturbations. However, for distributed sensing in harsh environments, the waveguide needs to be optimized as a sensing media and the coating on the optical fiber needs to provide mechanical protection at elevated temperatures. In this paper, we will review our work in three critical aspects of the optical fibers for sensing in harsh environments: waveguide design, coating thermal stability and mechanical strength at elevated temperatures.

Keywords: Distributed sensing, polyimide coating, optical fiber, high temperature, reliability, harsh environment

1. INTRODUCTION

1.1 Fibers for telecommunications and for distributed sensing

Since its inception more than 30 years ago, Distributed Fiber Optic Sensing (DFOS) has been widely recognized and gradually adopted as a critical sensing technology in many applications such as oil and gas sensing, pipeline leak detection, perimeter security and structural health monitoring [1,2]. Optical fibers optimized for DFOS in harsh environments differ in many ways from conventional fibers used in telecommunications. Conventional optical fibers for telecommunications are typically designed to transmit light signals in a protected environment, with nearly complete isolation from their surroundings, while sensing fibers are intended to sense changes in their environment.

More specifically, design for telecom fibers aims to ensure minimal levels of attenuation, optical non-linearity, macro and micro-bend losses, and other detrimental effects caused by external perturbations. Therefore the waveguide is optimized for transmission and is typically well protected by a dual layer acrylate coating system having a soft inner layer, a cushion to isolate the waveguide from micro-scaled perturbations in the fiber's immediate surroundings. However, for DFOS in harsh environments, in addition to being a waveguide, the optical fiber itself acts also as a sensor along its entire length, often requiring special coatings to shield itself from mechanical and chemical attacks in its environments while coupling certain environmental effects to the fiber core. Interestingly, many physical processes that enable fiber sensing are sometimes the very detrimental causes to be alleviated in the fibers for telecom. These can be Rayleigh scattering, Raman scattering and/or Brillouin scattering depending on the method of sensing. These optical scattering phenomena are affected by environmental conditions and, when harnessed deliberately, can be utilized in a distributed sensing fashion.

There are still many technical challenges, especially in fiber and sensor design optimization, waveguide and coatings materials characterization and selection, packaging for industrial applications and reliability engineering before DFOS fibers and cables will be considered a mature technology.

The following table summarizes some key differences in design considerations between the optical fiber for telecommunications and optical fibers for distributed sensing.

---

[*] jieli@ofsoptics.com; phone 1 860-678-6670; fax 1 860-674-8818; www.ofsoptics.com

Table 1. Comparison of telecom fiber vs. fiber for DFOS

Fiber Properties	Telecom	Sensing
Nonlinearities	Detrimental	Fundamental sensing mechanisms
Rayleigh Scattering	Minimized to lower attenuation	Benefit for acoustic sensing
Cutoff Wavelength	Designed for 1310 nm and 1550 nm	Optimized for operating wavelength
Bandwidth	Optimized for 850nm and 1310nm	Optimized for operating wavelength
Temperature	-40 to 85°C	-196 to > 300°C
Coating designs	To isolate the waveguide from its environment	Optimized for sensitivity to changes in fiber's environment
Mechanical properties and reliability	Well understood and proven	Incomplete

Since DFOS fibers are used for sensing, there are several design variables that should be optimized differently for sensing as opposed to transmission only. For instance, the cutoff wavelength for a single mode sensing fiber could be selected to be only slightly lower than the operating wavelength to enhance the confinement of the optical power with fiber core material, and hence the light-glass interaction, such as Brillouin scattering. Another example that we will discuss further in this paper will be the bandwidth performance of a multimode fiber that could be optimized for the sensing operating wavelength to improve spatial resolution and temperature resolution for a Raman Distributed Temperature Sensing (RDTS) solution. There are also unconventional fiber designs, such as dual-core fiber, that would significantly simplify the engineering efforts required with sensor packaging, installation, calibration and integration into sensing systems. We will discuss dual-core fiber further. Additionally, there are new and innovative sensing concepts and principles for distributed optical fiber sensing that are being continuously proposed and developed, such as enhanced Rayleigh scatter fiber sensing [3] and opto-mechanical sensing [4].

1.2 Coating thermal stability

For harsh environment applications, the coatings often become a factor that limits fiber's performance and long term reliability. Coatings on the optical fiber were originally invented to reduce fatigue, reduction in strength over time, to a point where silica glass fiber can maintain its strength for periods of 20 years or more. However, when used outside the limits of the environmental requirements for telecom, the coatings need to be capable of providing mechanical protection to the glass surface underneath it to preserve fiber strength, especially at elevated temperatures. Temperature is considered a most challenging variable for DFOS in harsh environments and the coating's thermal stability may determine the viability of the fiber in its final application.

There seems to be some confusion about how a coating's temperature rating should be defined. To help clarify, we proposed a definition for thermal stability of the fibers that ties the changes in coating material property with changes in fiber performance at elevated temperatures [5]. This approach allows quick evaluation and prediction of lifetime of fibers at elevated temperatures.

With an effective approach established, evaluation of coatings has now become straightforward. Consequently, it becomes possible to address the issue of lifetime for the fibers used in a non-telecommunications environment. Within this framework, we will describe a newly developed polyimide coated fiber capable of withstanding significantly higher temperatures.

1.3 Fiber mechanical performance at elevated temperatures

Key questions around performance remain. Even if the coating is stable at an elevated temperature, are common theories for optical fiber still applicable? What are some other factors contributing to the integrity of the fiber at elevated temperature? Unfortunately, existing theories and models for the silica fiber strength and fatigue would not be able to answer these questions as they were mainly developed for telecom applications where conditions are more benign. To help resolve this, we have conducted mechanical testing of fibers while exposing them to elevated temperatures and will discuss our findings on this subject.

In short, we will review our recent work in three critical aspects of the optical fibers for sensing in harsh environments: waveguide optimization and design for sensing, coating thermal stability, and mechanical strength and fatigue of optical fibers at elevated temperatures.

2. FIBER DESIGN FOR SENSING

2.1 Graded-Index multimode fiber (GIMM) with bandwidth optimized for DTS at 1550 nm

Raman-based distributed temperature sensing (RDTS) has become an essential tool in oil & gas production, pipeline monitoring, fire detection, heat tracing, industrial process monitoring, transportation monitoring, and monitoring of power transmission lines, etc. [6]. The RDTS systems are capable of achieving high temperature measurement accuracy of 0.1 °C, spatial resolution of less than 0.5 m, and distributed measurements over ranges exceeding 30 km [6, 7].

GIMM 50/125 optical fibers are the de facto choice for RDTS. However, commercially available GIMM optical fibers are designed for data communications at wavelengths of 850 nm and 1300 nm with highest bandwidth associated with such wavelengths commonly used for data transmission. For example, the bandwidth of an OM4 fiber at 850nm can reach several GHz·km. However because of the material dispersion, the value becomes much lower at wavelengths far away from the designed wavelength. Often, sensing systems operate at wavelengths other than 850 or 1300 nm. As such, accuracy and spatial resolution may suffer unless the waveguide is optimized for best use at the operating wavelength of the sensing system itself.

Some RDTS systems are designed to operate at 1550 nm to take advantage of the much lower fiber attenuation in this wavelength region. Doing so achieves better temperature accuracy and takes advantage of lower cost components commercially available at 1550 nm. However, if standard GIMM optical fibers are used for RDTS at 1550 nm, the intermodal dispersion will cause significant pulse broadening, limiting spatial resolution to a few meters. For many applications, this may not be acceptable.

Our solution is to design a GIMM fiber with the optimized bandwidth at 1550 nm. The refractive index profile is modified to minimize intermodal pulse broadening at 1550 nm based on theoretical predictions. For a GI MM fiber with cylindrical symmetry, the refractive index $n(r)$ of the core can be described by the equation below:

$$n(r) = n_c \sqrt{1 - 2\Delta \left(\frac{r}{a}\right)^{\alpha}}$$

$$\Delta = \frac{n_c^2 - n_{cl}^2}{2n_c^2} \qquad\qquad (1)$$

Where r is the distance from the center of the core; a is the core radius; n_c and n_{cl} are the refractive indices at the center of the core and at $r = a$, and $\pm$ is the profile exponent.

The intermodal pulse broadening of the GIMM fiber with such index distribution has been studied since the 1970's, and the bandwidth of a GI MM fiber can be theoretically predicted [8, 9]. The bandwidth, which is inversely proportional to pulse broadening, depends on the α value, wavelength, material dispersion and index difference (Δ) of the fiber. However, minimum pulse broadening can be achieved at each wavelength with an optimum α value. For example, for a GIMM fiber with a numerical aperture (NA) of 0.2, the optimum α is 2.027 at 850 nm and 1.871 at 1550 nm. The calculated root mean square (RMS) pulse width with α=2.027 and 1.871 vs. wavelength is plotted in Figure 1 to show the dependence of the pulse broadening on $\pm$ and wavelength. It is evident that if we use a GI MM fiber optimized for 850 nm at 1550 nm, the pulse broadening is an order of magnitude greater than that of a fiber optimized for minimal pulse broadening at 1550 nm.
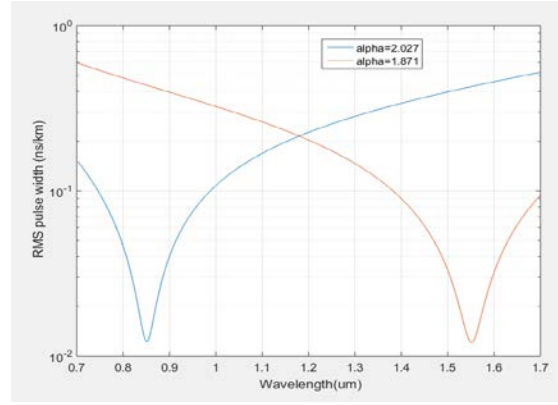
Figure 1. The calculated RMS pulse broadening with α=2.027 and 1.871

The idea was experimentally demonstrated by producing and testing a fiber with an index profile having ± equal to 1.871. The resultant bandwidth at three wavelengths is plotted below in Figure 2.
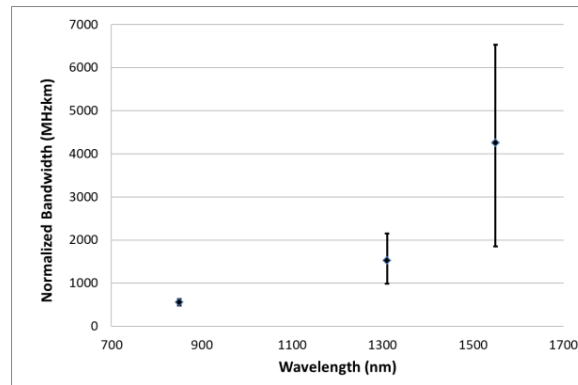

Figure 2. The measured bandwidth at 850 nm, 1310 nm and 1550 nm

The median of the measured bandwidth at 1550 nm is 4255 MHz·km while it is 560 MHz·km at 850 nm. The minimum bandwidth is 1800 MHz·km at 1550 nm, which is significantly higher than few hundred MHz·km for an OM4 MM fiber.

To test the fiber performance in an RDTS, the pulse broadening at 1550nm with 32 km of the GIMM fiber was measured and compared with 32 km of conventional OM4 fiber. The input pulse, with a 10 ns pulse width, and the output pulses after the 32 km of both fibers are plotted in Figure 3. Pulse broadening is confirmed to be less than 2 ns for the new GI fiber while performance-limiting pulse broadening is ~40 ns for the conventional OM4 fiber.
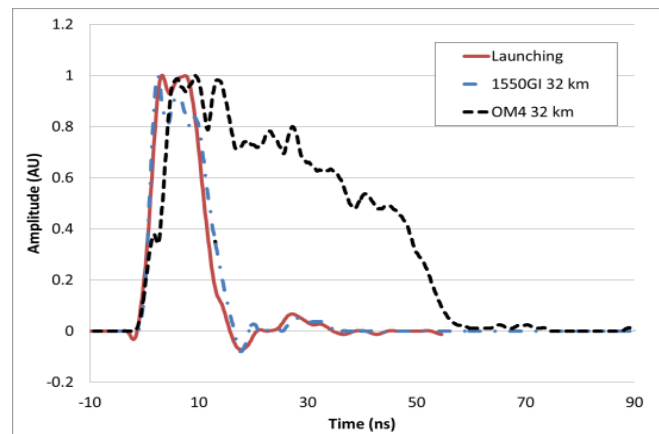

Figure 3. Comparison of measured output pulse shape from the new fiber and a standard OM4 fiber
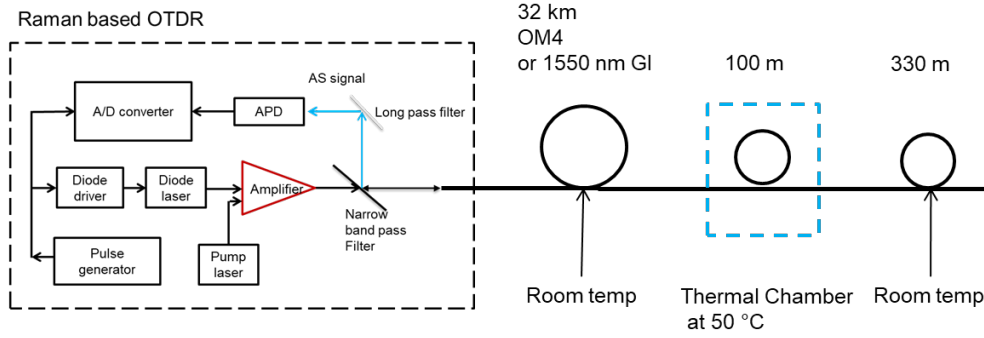
Figure 4. Test setup for RDTS measurement to determine spatial resolution.

The improvement of spatial resolution is then demonstrated in an RDTS measurement. The anti-Stokes signals with 32km of OM4 fiber or the bandwidth optimized GI fiber were acquired in a test setup shown in Figure 4 where a section of 100 m of fiber was heated to 50°C in a thermal chamber and the temperature distributions were calculated. The calculated temperatures vs. distance near the input of the 100 m fiber kept in the chamber are shown in Figure 5. The fiber temperature is transitioning from room temperature, right outside the thermal chamber, to 50°C, inside the chamber, and the spatial resolution can be readily calculated for this transition. The spatial resolution is defined as the measured spatial distance between the 10% and 90% levels of the response to a step temperature change. Based on the temperature traces shown in Figure 5, the spatial resolution is 3 m at 32 km for the 1550 nm bandwidth optimized GIMM fiber while it is 10 m at 32 km for the OM4 fiber. The spatial resolution is improved by more than a factor of 3 and this is realized simply because the increased bandwidth at 1550 nm enables small pulse broadening after 32 km of fiber.
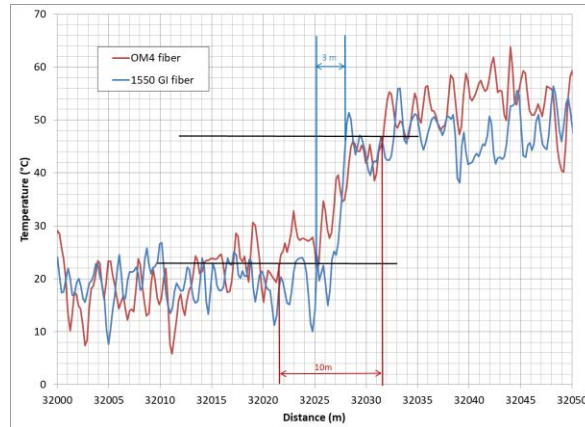

Figure 5. The experimental DTS measurements near the input of the 100 m length of fiber in the thermal oven.

In summary, we have designed and manufactured a new GIMM optical fiber that enables minimum intermodal pulse broadening at 1550 nm. Using the fiber at 1550 nm, we have demonstrated a spatial resolution of less than 3 m after 32 km of the fiber in RDTS measurements, an enhancement of a factor of 3 as compared with the resolution achievable with a conventional OM4 fiber.

2.2 Dual multi-mode core fiber and sensor for DTS

RDTS uses the principles of Optical Time Domain Reflectometry (OTDR) to measure the Raman backscattering originating along the length of the fiber. RDTS then computes the ratio of the intensities of Anti-Stokes and Stocks backscattered peaks to determine temperature changes in a distributed way [10]. As the Anti-Stokes peak is more temperature sensitive than the Stokes peak, the measurement of the ratio enables the measurement of the temperature. Since the wavelength difference between the Stokes and Anti-Stokes peaks can be greater than 100 nm, the optical losses at these two wavelengths, wavelength dependent loss (WDL), could be problematic over a long length of fiber. This often leads to significant error in temperature measurement. WDL can be caused by Rayleigh scattering linearly

distributed within the fiber, limited number of fiber splices and connectors, unpredictable stresses along the length of the fiber and sometimes hydrogen or radiation induced loss in the optical fiber.

Several methods have been used for WDL associated error in DTS, such as the two light source approach [11], a method that uses a high reflection mirror at the far end of the fiber [12], and dual-ended systems [13]. Among all of these methods, the dual-ended systems are more attractive as they can automatically correct errors caused by WDL, although the light path length required is two times that of the single-ended method. Dual-ended systems often lead to more complicated installation process, especially when the two independent fibers may need to be installed separately and field-connected at the distal end in order to create the dual-ended light pathway.

In a typical dual-ended system, two individual optical fibers are laid parallel to each other and are connected at the distal end so that light can be launched into each leg at the proximal end. The connection at the distal end is typically made by bending a short length of fiber and splicing the short fiber with the two lengths of sensing fiber together, forming a U-shaped optical path. The short U-shaped section of the fiber is then packaged and sealed inside a glass capsule. However, there are several disadvantages associated with this design. Aside from the optical loss induced by the tight bend, mechanical stresses caused by the bend could limit the lifetime of the device. Furthermore, bulky size of the glass protective capsule around this "bend" may interfere with packaging and installation of the finished sensor, especially in applications with confined spaces,

We have taken the approach of optimizing design of the fiber and fiber-based components for RDTS sensing applications. Rather than making a sensor using existing fiber, we have designed a single fiber sensor for dual ended system using 1) a dual-core fiber with 2) a miniaturized, matched diameter, solid-state turn-around device, known as a micro-turnaround, built with a graded index (GRIN) MM fiber and 3) a fan-out device and demonstrated the sensor in dual-ended RDTS.

The dual-core fiber consists of two 50 μm multimode cores, identical to the cores for the 50/125 GIMM fibers commonly used for DTS, spaced 100 μm apart, as shown in Figure 6. Its outer glass cladding diameter is 200 μm, allowing greater separation between the cores to minimize the crosstalk. The large spacing between the cores also simplifies its connection to two individual single-core GI MM fibers in a fan-out device. The fiber is coated with dual acrylate coating to a 350 μm diameter.
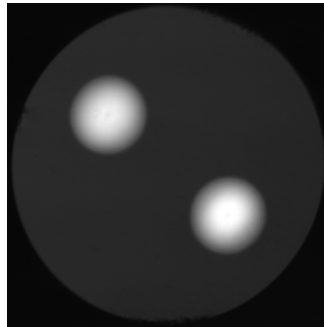

Figure 6. End-face image of the dual-core fiber taken by an optical microscope with the fiber illuminated from both ends

Low optical crosstalk between the two cores is important for the dual-core fiber as high crosstalk could create errors in the temperature measurement. Crosstalk is related to factors such as spacing between the cores, core diameter variation, scattering and fiber bending. We used fiber bending to induce worst case crosstalk utilizing a 2-point bend device. A long dual-core fiber, 2.63 km in length, was coiled onto a 10-inch spool with fan-out devices spliced to both ends of the fiber. 1064nm light was launched into one core at the input end and the power from both cores was measured at the output end. The crosstalk is defined as $crosstalk = 10 \cdot \log(P2/P1)$ where $P1$ is the measured power exiting from the core in which the light was launched, and $P2$ is from the other core, or second half of the light's pathway. A section of the dual-core fiber near the output end was put into a 2-point bend device to bend the fiber at 180 degrees for worst case crosstalk inducement. The cross talk result is shown in Figure 7.
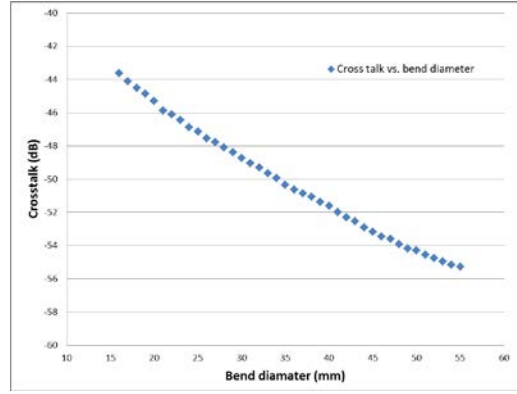
Figure 7. Crosstalk vs. bend diameter at 1064nm.

The micro-turnaround device used here measures less than 300 µm in diameter and less than 2 mm in length. The distal end of a dual-core based fiber sensor with a micro-turnaround (darker section) is shown together with a conventional fiber bend device with two fibers in Figure 8.
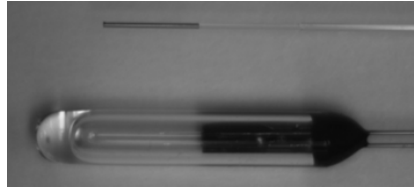

Figure 8. Images of the micro-turnaround (Top) and the fiber bend device (Bottom).

As illustrated in Figure 9, the left side represents the dual-core fiber while the right side represents a GRIN fiber lens with a high reflectance coating applied to its end face. The cladding diameter of the GRIN fiber lens in our experiment is 200 µm to match that of the dual-core fiber, as shown in the top half of the photograph in Figure 2.
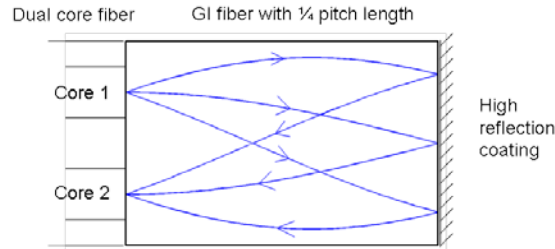

Figure 9. Illustration of dual-core fiber turnaround.

The index distribution of the GI fiber lens can be described as [14]:

$$n(r) = n_0(1 - \frac{g^2}{2}r^2) \tag{2}$$

where r is radial distance from the center, n_0 is refractive index at the center of the GRIN fiber, and g is the gradient. The gradient g is related to the measured NA and the core size a by:

$$g = \frac{NA}{a \cdot n_0} \tag{3}$$

A beam propagating in the GI medium follows a sinusoidal path, and the pitch or period of the sinusoidal path [14] is:

$$P = 2\pi / g \tag{4}$$

With a high reflection mirror placed at the ¼ pitch position, the input from one core will be mirrored to its opposing side (opposite core) with a 1:1 ratio in dimension. We illustrate this in Figure 4 with the traces calculated using a ray tracing method. The light exiting from Core 1 will expand and become collimated by the GRIN fiber lens, be reflected by the mirror and then be focused back onto Core 2, completing the desired turnaround path. The core diameter of the GRIN fiber lens is 180 µm and the NA is 0.275 with the calculated ¼ pitch length ~757 µm based on equation (3).

To connect between the dual-core structure and two individual single-core multimode fibers, fan-out devices were designed and made with commercially available GI 50/125 fibers and the dual-core sensor fiber. The fan out has an insertion loss of <0.5dB from 850nm to 1300 nm, and a crosstalk <-60dB. The dual-core end of the fan-out can be spliced to the dual-core fiber using commercially available fusion splicers designed for polarization maintaining (PM) fiber splicing, and the splicing loss of the two cores is typically <0.1dB.

After optically characterizing the sensor, the dual-core fiber is tested in an RDTS experiment. The experimental set up is shown in Figure 1, where a section of the fiber sensor is placed in a thermal chamber heated to various temperatures with lead-in and tail sections of the sensor placed outside of the thermal chamber.
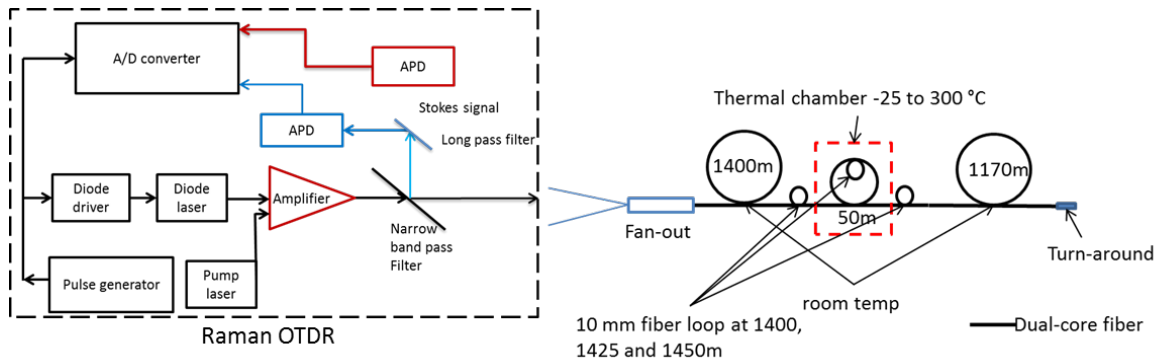

Figure 10. Setup for distributed temperature measurement with dual-core optical fiber

The sensor fiber used for the thermal test had two 50 µm GI cores with 100 µm separation and a glass cladding diameter of 225 µm. This fiber was further coated with a polyimide coating (high temperature) to a diameter of 260 µm in order to work at elevated temperature up to 300°C. A fan-out was spliced to the dual-core fiber to couple light in and out of the two individual cores. The output fiber from the Raman OTDR could be spliced to either of the two 50/125 GI fibers to interrogate the dual-core fiber in either forward or backward direction. A micro-turnaround device [17] was spliced to the end of the dual-core fiber to form a complete turnaround loop.

The total length of the dual-core fiber was 2620 meters (m). A 50 m section from the middle of the fiber was put in a thermal chamber and the rest of the sample were kept at room temperature (around 16°C) as reference as shown in Figure 10.

During the test, the temperatures was set to, -25°C, 50°C, 100°C, 200°C and 300°C respectively, and the Stokes and Anti-Stokes signals were obtained from either end of the fan-out alternatingly. The ratios of the Anti-Stokes to Stokes intensities were then calculated to determine the temperature distribution of the fiber. The measured temperature distributions are shown in Figure 11 (a) with an enlarged view for the 50 m section shown in Figure 11 (b).
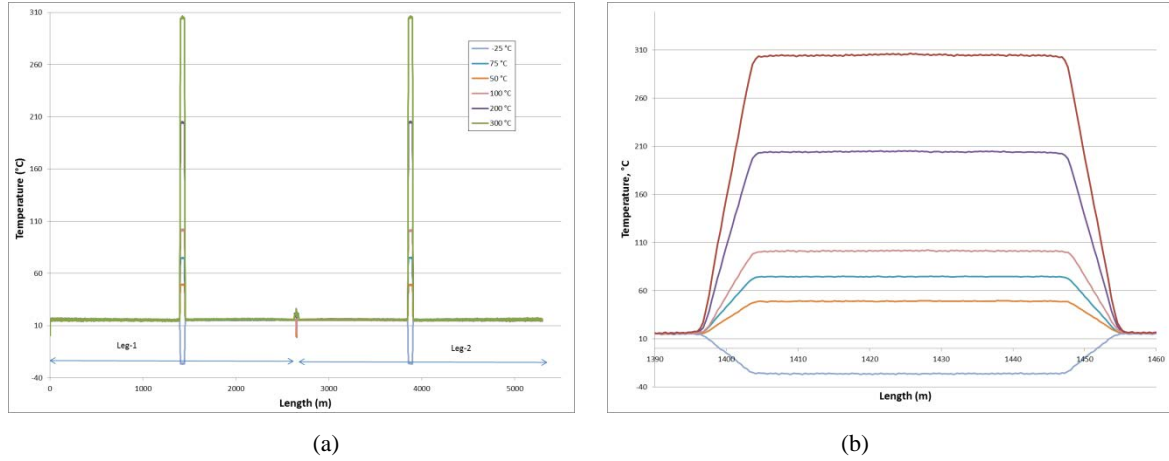
Figure 11. (a) the measured temperature profile of the dual-core fiber with a micro turn-around device; (b) measured temperature around the 50 m section in thermal oven and the Stokes signal with the fiber at the room temperature.

We have designed a dual core fiber based DTS sensor with miniaturized turnaround, and a fan-out device and have demonstrated its advantages in a distributed RDTS measurement. This single fiber, dual-core design with a micro-turnaround is self-calibrating, significantly simplifies the engineering effort required for installation and improves the reliability of the sensor.

3. THERMAL STABILITY OF FIBER COATINGS

Logically, for optical fibers used in DFOS, coating systems will also need to ensure proper level of coupling of the changes in physical variables from the environment to the fibers as the sensing media, such as strain coupled from the environment to the fiber core in a strain sensing fiber. However, we concentrate our work here on the basic role of the coatings, that is, to provide mechanical protection to the fiber, especially in harsh environments.

There are several factors that define the harshness of the environments for the fiber coatings in DFOS: (1) Physical environment that the fiber coatings are in direct contact with, such as, inside a stainless steel tube or a conduit, in a composite material, and other packaging configurations); (2) Chemical environments, such as in water, oil, vapor, acids, bases, and hydrogen containing gas or liquid; (3) exposure temperature and (4) exposure pressure. In this work, we focus on the impact of elevated temperatures on the fiber, as it is the most common and challenging variable encountered in harsh environments.

Thermal stability of the coatings that are protecting the fibers dictate the thermal stability of silica optical fibers with these coatings since silica glass is more thermally stable than polymer coatings used for optical fibers. All polymer coatings start to experience a gradual process of thermal decomposition when the environment provides a sufficiently high amount of thermal energy. As the molecules of the polymers are being gradually released into the atmosphere through thermal decomposition, the coating experiences the irreversible process of weight loss, manifested by the diameter reduction of fiber coating itself, change in coating modulus and coating deformation. The changes in the coating lead to weakening and eventual mechanical breakage of the coated fiber. Therefore the challenge for reliable use of fibers is to develop a coating that protects the fiber at the desired temperature for the intended duration.

3.1 TGA and thermal stability

If the thermal weight loss of polymer materials is considered the main failure mechanism, the thermal stability or temperature rating of the fibers protected with these coatings should be defined by both temperature and duration. To quantitatively evaluate the thermal stability of the fibers coated with different coatings, we proposed an approach that ties fiber failure with coating property changes [5, 16]. In this method, thermogravimetric analysis (TGA) of coated fiber samples is coupled with a test of the coated fiber for a specific failure mode at corresponding temperatures. More specifically, first, an interested failure mode and its criterion are selected. For example, the failure mode could be induced-optical attenuation, loss of mechanical strength, cracking or discoloration of the coating, and loss of volatile compounds, etc. Once the failure mode and its criterion are defined, the fiber is aged at a preset elevated temperature until this failure is observed as in the middle section of Figure 12 to determine its lifetime at elevated temperatures. A

TGA experiment is performed for the same temperature range to determine the corresponding weight loss of the coating at the time of the fiber failure as indicated by the lower section in Figure 12. In this way, the failure mode of an optical fiber is linked with a TGA weight loss, which can be treated as the failure TGA weight loss for the specific fiber failure mode.
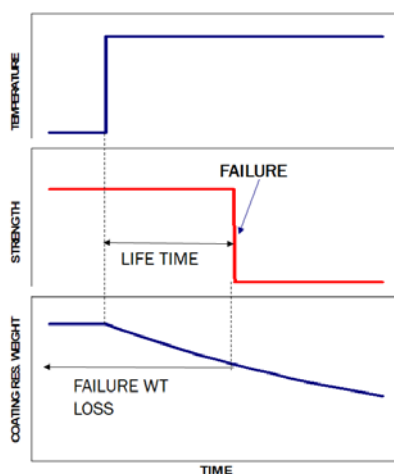

Figure 12. Explanation of the TGA approach.

The TGA data collected isothermally at different temperatures or non-isothermally at different heating rates can be used for evaluating the times and temperatures that correspond to the failure weight loss and then extrapolated to lower or higher temperature regions with longer or short lifetimes. Another use of the method is to compare the thermal stability for different coatings. For instance, we may select an arbitrary failure criterion of 25% of the coating weight loss for an arbitrary failure mode. Examples of the results obtained for fibers coated with dual acrylate, silicone and polyimide coatings are shown in Figure 13. Extrapolation of the data to 20-year lifetimes yields the following upper use temperatures: ~90°C for the dual acrylate coating, ~125°C for single acrylate; ~160°C for silicones and ~245°C for traditional polyimides.
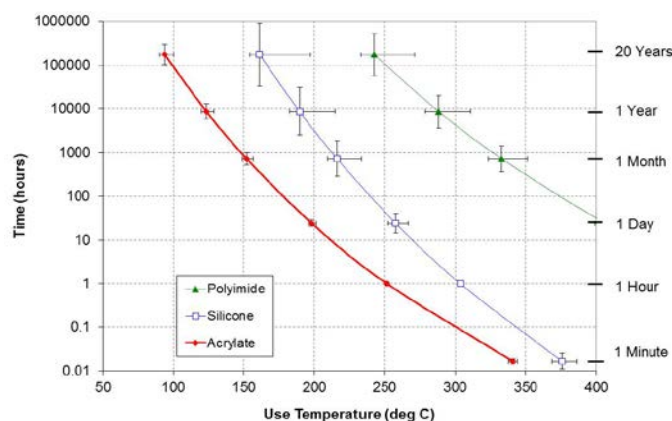

Figure 13. Continuous usage time plotted vs. temperature for fibers with dual acrylate, silicone and polyimide coatings in air environment. The data are based on TGA analysis assuming 25% weight loss criterion.

3.2 Pyrocoat K

Building on this foundation, we recently developed a polyimide coating with enhanced thermal stability, Pyrocoat K. For this coating, the upper use temperature with 20 year lifetime is ~293°C [17], enabling a possible solution to a very specific issue for the polyimide coating at elevated temperatures. Above 250°C, typical polyimides approach their glass transition temperature and become "sticky". In practice, such polyimide-coated fibers adhere to most surfaces they contact, such as the inner wall of a Fiber-In-Metal-Tube (FIMT), commonly used for fiber packaging in oil and gas

sensing. Subsequent cooling of the FIMT may lead to mechanical breakage of the fiber due to a breach in coating and or a CTE mismatch between the metal and silica glass.

To evaluate the issue of stickiness of polyimide-coated fibers to metal, the following experiment was performed. Pieces of polyimide-coated fiber were bent into a U-shape and inserted into ¾'' ID stainless steel tubes. The specimens were then places in a thermal oven and kept at 300°C for 24 hours. After cooling to room temperature, it was observed that the fibers adhered to the inner wall of the stainless tube and could not be removed from the tubes without breaking the optical fibers. Figure 14 shows a piece of stainless steel tube hanging onto the fiber that is stuck onto its inner wall. Similar experiments were performed using fibers coated with the Pyrocoat K polyimide. This coating was designed to be less sticky to metal surfaces and Pyrocoat K coated fibers exhibited no adhesion to the stainless steel tube with identical 300°C exposure.

This experimentation has practical implications as it solves a significant reliability problem for those using optical fibers within metal tubes for high temperature sensing.

Figure 14. A piece of stainless steel tube is hanging on a polyimide-coated fiber after exposure at 300°C.

We have described an approach to determine the thermal stability of the coatings that uses TGA and a test associated with a specific failure mode at elevated temperature. We also briefly described an important advantage of Pyrocoat K.

4. MECHANICAL STRENGTH AT ELEVATED TEMPERATURE

4.1 Fiber strength at elevated temperature

As discussed earlier, the polymer coatings that protect optical fibers are the limiting factor for mechanical behavior of such fibers at elevated temperatures. However, when the coating is not compromised, it is not clear that the fracture mechanics and reliability predictions, applied successfully to silica glass fiber at ambient (-40 to +85°C) temperatures, are still applicable at elevated temperatures like those seen in harsh environment sensing. To ensure the reliable use of silica optical fiber as a technology with higher level of readiness for DFOS at elevated temperatures, the mechanical properties and lifetimes need to be fully understood and characterized. However, very little research has been published on testing fiber for mechanical properties while at elevated temperatures. Most studies have been conducted at ambient temperature on the fibers that were exposed to elevated temperatures, rather than tested at actual elevated temperatures. In this work, we demonstrate a test setup to characterize fiber mechanical properties, strength, and fatigue resistance, at elevated temperature. We obtained interesting results that are meaningful to the harsh environment application of optical fiber.

To test fiber strength at elevated temperatures, a standard tensile tester was modified by adding a furnace to heat the sample while straining the sample until its fracture as shown in Figure 15. The temperature inside of the furnace was maintained at the desired temperature during the test. The fiber sample was held vertically and wrapped on capstans at both ends. The fiber sample was pulled vertically by a moving capstan at a constant strain rate. Four different strain rates (28%/min, 4%/min, 0.57%/min and 0.08%/min) were used to investigate the dynamic fatigue behavior. The gauge length for the test was 0.85 m. The entire setup was maintained in a controlled ambient environments (RH = $50 \pm 5\%$, T = $23 \pm 2°C$) [18].
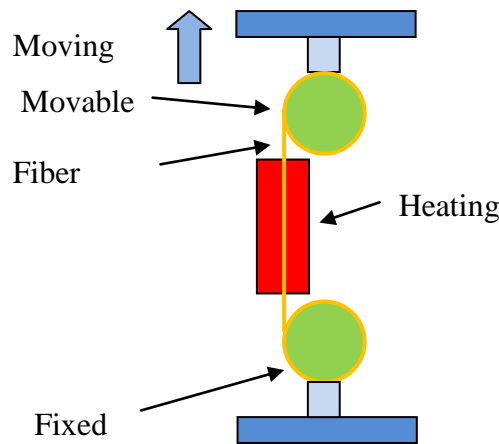
Figure 15. A schematic of a Stationary Capstan Fiber Tester (SCFT) with a heater for the fiber under test.

The fibers used for the test are polyimide coated fibers having a 125 μm silica glass cladding, and a coating diameter of 155 μm. For comparison, fibers having a commercially available dual acrylate coating were also used.

4.2 Weight loss data as a function of heating temperature

Since the coatings are the limiting factor, TGA analysis was carried out on the polyimide-coated fiber together with the acrylate coated fibers. Figure 16 represents a typical dynamic TGA curve collected at a heating rate of 0.5 ℃/min for polyimide coated fiber in air, along with the curve for a standard fiber with dual-acrylate coating for comparison.
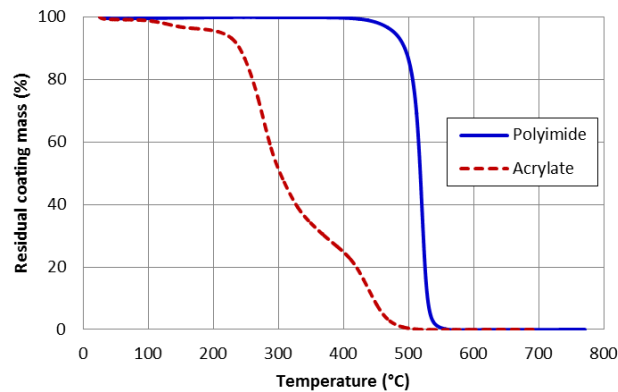

Figure 16. Dynamic TGA curves obtained for polyimide coating (blue solid line) and dual-acrylate coating (red dashed line) in air at a heating rate of 0.5 ℃/min.

As can be seen, the polyimide coating does not exhibit significant weight loss below 400 ℃ while the acrylate coating starts decomposing below 200 ℃.

4.3 Weight loss data as a function of heating duration at 350 °C

To access weight loss as a function of time at a given temperature, an isothermal TGA experiment was carried out. The fiber samples were heated to 350°C at 75°C/min and then kept at the temperature for 24 hours while the sample weight was recorded. The result is presented in Figure 17. At 350°C, the polyimide coating lost about 2% of its initial weight upon heating and no significant weigh loss was observed in the 24 hour period. The initial 2% weigh loss may include the loss of volatiles (water and residual solvent) only. In comparison, a dual-acrylate coating loses about 90% of its initial weight during same exposure.
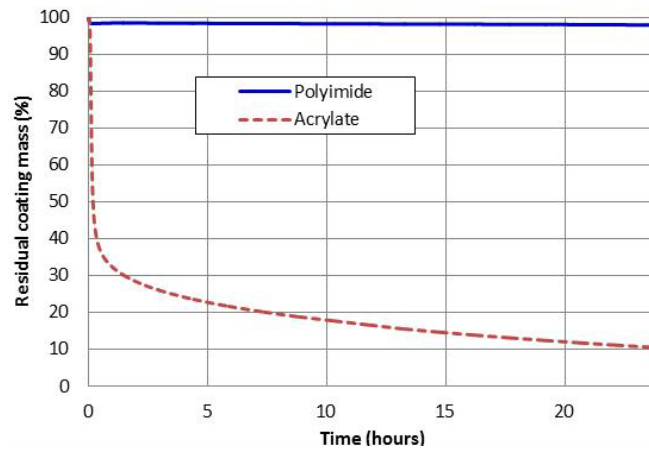
Figure 17. Isothermal TGA curves obtained for polyimide coating (blue solid line) and dual-acrylate coating (red dashed line) in air at 350 ℃.

4.4 Mechanical strength at elevated temperatures

Fiber samples were loaded into the tensile tester first before the heating started and the actual testing began once the temperature stabilized at the set point, which took typically a few minutes. We selected 350℃ as the temperature for the dynamic tensile study. The fiber strength after 60 minutes soaking at 350 ℃ decreased slightly and the data set variance became greater, as shown in Figure 18.
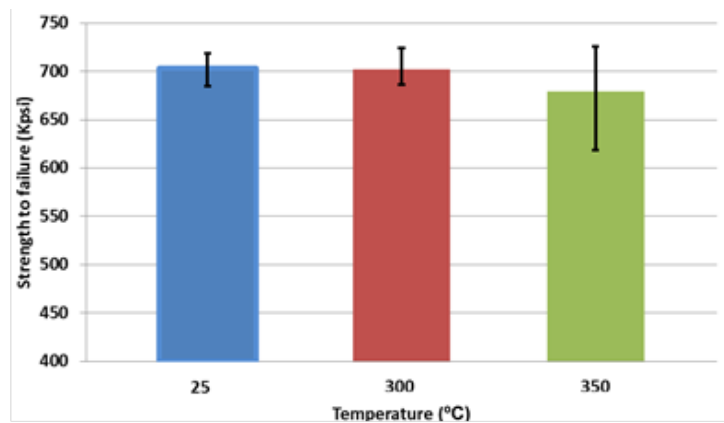

Figure 18. Dynamic tensile strength results of polyimide coated fiber at room condition (blue bar on the left), 300 ℃ for roughly 10 mins exposure (red bar, middle) and 350 ℃ for roughly 60 mins exposure (green bar, right), respectively. The data points correspond to medians while the error bars show the maximum and minimum observed values.

The resultant fiber strength didn't decrease drastically with the temperature increase from room temperature to 350℃. Our data seemed to suggest that the intrinsic properties of the glass responsible for fiber strength remain unchanged as long as the coating remains intact and continues to provide sufficient protection. This is supported by the TGA data for polyimide coated fibers illustrated in Figs. 16 and 17.

In an earlier study an Arrhenius model proposed predicted a strong temperature dependence of the strength of silica fiber in the temperature from 77 to 473 K [19]. In the same paper, both bare glass fiber and metal coated fibers were studied for strength in a temperature range from room temperature to 200°C. The measured strength was observed to decrease significantly as the temperature increases, suggesting strong temperature dependence.

A possible explanation for our observation is that we used polyimide fiber and the thermal stress created on glass due to the coefficient of thermal expansion mismatch of silica and polyimide is much less than that between glass and metal coating used in the earlier study [19].

4.5 Dynamic tensile strength as a function of time

To access the impact of aging at elevated temperature, samples were soaked at 350°C at different duration and then tested at 350°C. The results are displayed in Figure 19. A significant decrease in strength and increase in data variance were observed after 24 hours of thermal aging. This decrease in strength is inconsistent with the TGA data shown in Figure 4, which indicates no significant weight loss for polyimide coating at 350°C up to 24 hours. After examining the sample surface, we observed that while TGA results provide average material properties of the coating, they do not offer information on localized changes caused by localized higher temperatures in the coating. This degradation in fiber strength is suggested to be caused by a different mechanism of the coating, such as the formation of the surface defects.
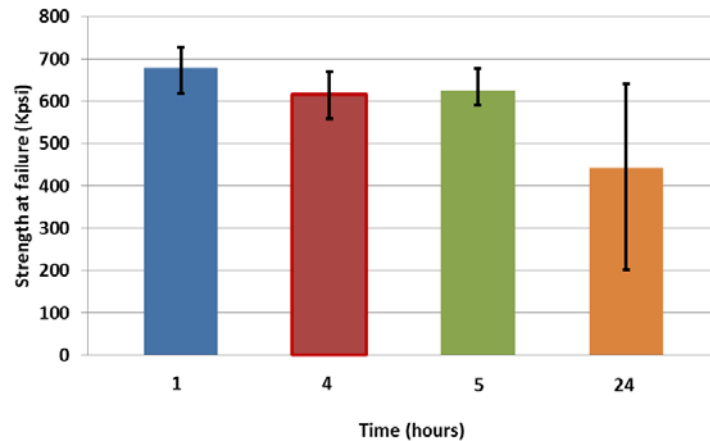

Figure 19. Dynamic tensile strength results of polyimide coated fiber at 350°C for dwell time of 1 hour (blue bar), 4 hours (red bar), 5 hours (green bar) and 24 hours (orange bar), respectively. The data points correspond to medians while the error bars show the maximum and minimum observed values.

4.6 Observation of changes in surface morphology

In an earlier study [20], the formation of crater-like defects was observed on the coating surface of polyimide-coated fiber samples treated at elevated temperatures. It was theorized that the craters were initiated at the locations of small-scale debris on the coating surface. These defects were identified as root cause for weak mechanical performance of the fiber under study. The research concluded that the craters could reach the glass surface leaving it unprotected and subsequently triggering critical crack growth, resulting in fiber fracture. This could be a possible explanation for the pre-mature fiber fracture at elevated temperatures where weight loss of the coating is insignificant.

To confirm the hypothesis, the following experiment was performed. Two sets of fiber samples were prepared with one set carefully surface-cleaned while the other set was intentionally subjected to dust as shown in Figure 20 (a) and (b). The samples were then placed vertically in a thermal oven and simultaneously aged in ambient air at 400 °C for 24 hours. It can be clearly seen in Figure 20 (d) that the craters developed on the "dusty" sample surface as consequences of combustible dust particles, such as fabric fibers, being "burned-off" and generating very high localized temperatures.

(a)   (b)

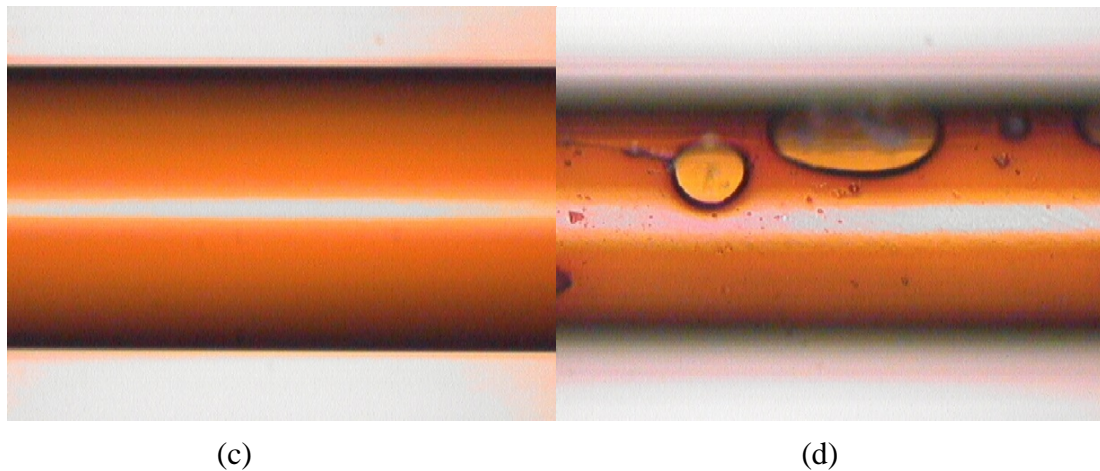<div align="center">(c)　　　　　　　　　　　　　　　　　　(d)</div>
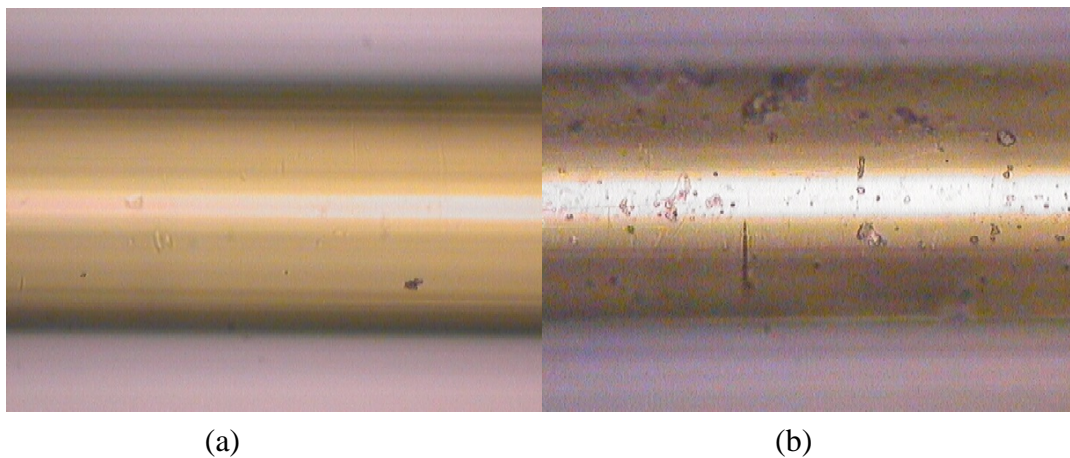
Figure 20. Microscope images of carefully cleaned polyimide coated fiber before (a) and after (c) 24 hour aging at 400°C, and "dusty" fiber sample before (b) and after (d) 24 hour aging at 400°C.

Following the aging experiments, two-point bend strength testing was carried out to examine the effect of these craters on strength. Strength data summarized in Table 2 suggest that these craters significantly degraded the mechanical strength of the fiber under test. Note the Weibull slope also changed from a baseline of 116 to 3.3, indicating a much more scattered strength distribution. It is believed that formation of such craters significantly reduces or eliminates the coating locally, exposing the silica glass surface to environmental moisture and significantly reducing the fiber strength.

Table 2. Two-point bend strength data of unaged, carefully cleaned and "dusty" polyimide fiber samples

Fiber sample	Median strength (kpsi)	Weibull slope
Unaged	828	116
Aged at 400 °C for 24 hours - cleaned	784	42
Aged at 400 °C for 24 hours - dusty	526	3.3

This observation provides an explanation for the decrease in strength of polyimide coated optical fibers at a temperature where no significant coating weight loss is observed. The greater scatter of the strength data can also be explained by the random nature of the distribution of dust particles on coating surface. A thorough cleaning step for the fiber samples has since been added to our test procedure.

4.7 Fatigue behavior at elevated temperatures

Following the strength tests, the fibers were tested to determine the fatigue resistance factor, the *n* value, at room temperature and 300°C using four different strain rates and the results are compared. For the tests at 300°C, the fiber samples were thoroughly cleaned, placed, and heated to the set point in the furnace. The tests started as soon as the temperature in the furnace stabilized. The duration of the fiber under test at 300°C varies from 20 seconds for the strain rate of 28%/min to 2 hours for the strain rate of 0.08%/min. Since the coating is stable at 300°C, the effect of heating duration on the test result should be minimal. The results are shown in Figure 21 and Figure 22.
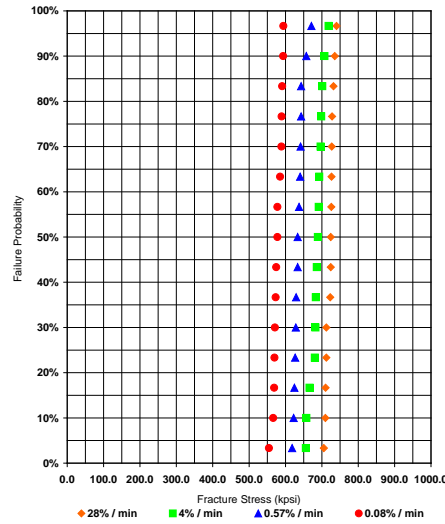
Figure 21. Weibull plots of polyimide coated fiber at four different strain rates at 300°C.
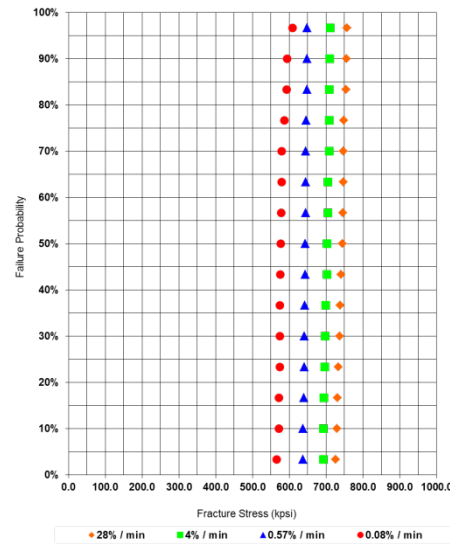

Figure 22. Weibull plots of polyimide coated fiber at four different strain rates at room temperature.

All plots for the polyimide coated fiber are nearly vertical, indicating a tight distribution or a desirable Weibull slope. The test results are also summarized in Table 3 for easy comparison.

Table 3. Mechanical tensile strength data of polyimide fiber samples at different strain rates at 300°C

Strain rates (%/min)	Median strength (kpsi) Room Temperature	Median strength (kpsi) 300℃	Weibull slope Room Temperature	Weibull slope 300℃
28	744	724	80	82
4	702	687	109	48
0.57	643	637	187	85
0.08	576	578	68	65

From the table above, median strength and slope both decreased only somewhat, indicating that the polyimide coating as a protection for fiber at elevated temperatures is very effective. The slight decrease could still be related to the cleanliness of the coating surface.

A strong dependence of fiber strength on strain rate is also evident in the results shown above, a behavior known as dynamic fatigue. Dynamic fatigue behavior of the fiber allows us to determine the fatigue resistant factor, the n value, experimentally. The fatigue resistance factor is calculated based well-established theories for glass fatigue using the following equation [21].

$$n = \frac{\ln(\dot{\sigma}_1) - \ln(\dot{\sigma}_2)}{\ln(\sigma_1) - \ln(\sigma_2)} - 1, \tag{5}$$

Where $\dot{\sigma}_1$ and $\dot{\sigma}_2$ are the different strain rates used, σ_1 and σ_2 represent fiber breaking stresses. Figure 23 and Figure 24 are the examples of obtaining n values based on the test data using the equation (5).
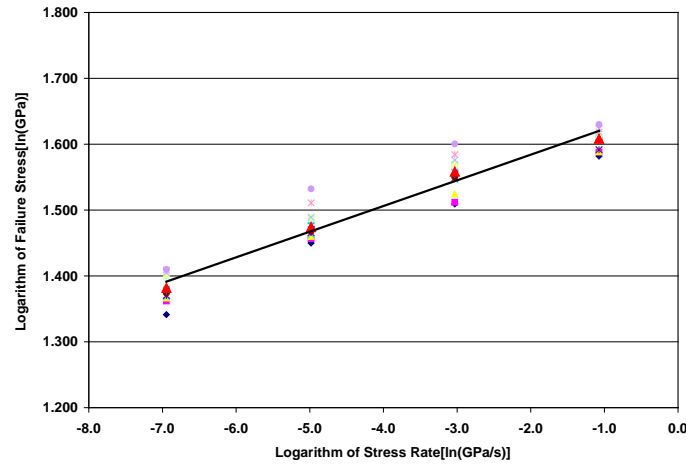

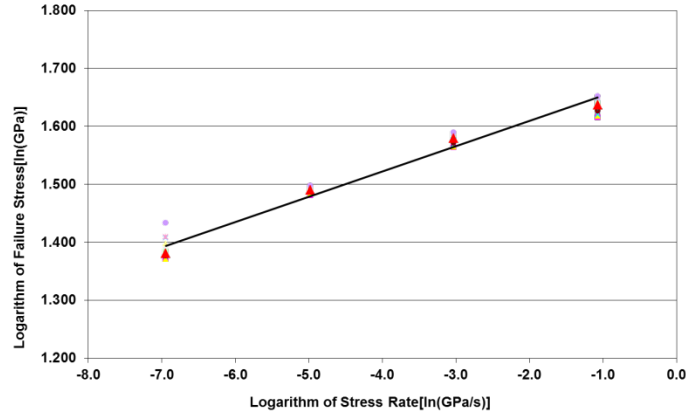Figure 23. Fatigue of polyimide coated fiber at 300°C and n_d = 25.4.

Figure 24. Fatigue of polyimide coated fiber at room temperature and n_d = 22.6.

The calculated n_d value for the fiber at 300°C is 25.4 while the n_d is equal to 22.6 for the data obtained at room temperature. Given the statistical nature of mechanical strength test and the sampling size, we may not be able to say anything more definitive. However, the data suggests that the fatigue behavior of the fiber under study did not degrade significantly at 300°C.

We have described our novel approach of testing fiber mechanical properties during elevated temperature exposure. The polyimide coated fibers under test performed unexpectedly well once the surface contamination was eliminated. It indicates that the glass fiber retains its mechanical behavior, strength and fatigue resistance, so long as the coating continues to protect the glass surface.

5. SUMMARY

In summary, we have reviewed our recent work on a number of topics:

1. Fiber and sensor designs

    a. Conventional GIMM fiber designs can be used as sensor, but, application dependent, will exhibit sensing performance limitations as they are optimized for data transmission, and not specifically intended for use in sensing applications.

    b. "sensing optimized" GIMM fiber with its bandwidth tuned for 1550 nm can provide significant improvement in the sensing distance and spatial resolution for RDTS applications.

    c. A dual-core GIMM sensing fiber with a micro-turnaround device and fan-out device provides optimization for dual-ended RDTS systems significantly simplifying the engineering efforts in deployment and improving reliability in confined installation space applications.

2. Coating thermal stability

    a. Coating and optical fiber reliability models to serve markets outside of the typical telecommunications temperature range (-40 to + 85°C) must be developed in order to provide DFOS solutions for harsh environments with reliability levels that are attractive for those markets.

    b. Pyrocoat K coating, highlighted in this paper, provides an example of how materials science is used in fiber optics to broaden the performance and reliability envelope for markets such as sensing in harsh environment.

3. Fiber mechanical behavior at elevated temperatures

    a. Polyimide coated fibers were tested while at elevated temperatures for mechanical strength and fatigue resistance.

    b. Formation of the crater-like defects was observed as a failure mode for fiber strength at the temperature the coating is stable. Surface cleaning is effective solution.

    c. The results showed performance stability as a function of temperature. This suggests that it is the integrity of the polyimide coatings at elevated temperatures, not the intrinsic glass properties, that determine fiber mechanical performance, strength and fatigue resistance.

To advance DFOS technology to a higher readiness level, our focus will continue to be in the areas of fiber and fiber based component designs, coatings and packaging materials development, reliability engineering and fundamental materials research.

6. ACKNOWLEDGEMENTS

REFERENCES

[1] Hartog, A. H. and D. N. Payne, "A fibre-optic temperature-distribution sensor," IEE Colloquium on Optical Fibre Sensors, London, IEE, Digest, 1982/60: 2/1-2/2.
[2] Arthur H. Hartog, "An introduction to distributed optical fibre sensors," CRC Press, 22-24, 2017
[3] P. S. Westbrook, et al, "Kilometer length, low loss enhanced back scattering fiber for distributed sensing," OFS-25, 1-5 (2017).
[4] Y. Antman, A. Clain, Y. London, and A. Zadok, "Optomechanical sensing of liquids outside standard fibers using forward stimulated Brillouin scattering." Optica, 3(5), 510 – 516 (2016).

[5] A. A. Stolov, D. A Simoff, J. Li, "Thermal stability of specialty optical fibers," *J. Lightwave Technol.*, 2008, V 26, N 20, P. 3443-3451.

[6] Bao X. and Chen L., "Recent progress in distributed fiber optic sensors," Sensors 12, 8601–8639 (2012).

[7] A. Signorini, S. Faralli, M. A. Soto, G. Sacchi, F. Baronti, R. Barsacchi, A. Lazzeri, R. Roncella, G. Bolognini, and F. Di Pasquale, "40 km long-range Raman-based distributed temperature sensor with meter-scale spatial resolution," OFC 2010

[8] R. Olshansky and D. B. Keck, "Pulse broadening in graded-index optical fibers," Appl. Opt. 15, 483 (1976).

[9] Katsunari Okamoto, "Fundamentals of Optical Waveguides", Academic Press, pp 108-117 (2005)

[10] J. P. Dakin; D. J. Pratt; G. W. Bibby; J. N. Ross, "Distributed optical fiber Raman temperature sensor using a semiconductor light source and detector," *Electron. Lett.* **21**(13), 569–570 (1985).

[11] K. Suh; C. Lee, "Auto-correction method for differential attenuation in a fiber-optic distributed-temperature sensor," *Opt. Lett.* **33**(16), 1845–1847 (2008).

[12] Hwang, D.; Yoon, D.-J.; Kwon, I.-B.; Seo, D. C.; Chung, Y., "Novel auto-correction method in a fiber-optic distributed-temperature sensor using reflected anti-Stokes Raman scattering," *Optics Express*, **18**(10), 9747–9754 (2010).

[13] Fernandez, A. F.; Rodeghiero, P.; Brichard, B.; Berghmans, F.; Hartog, A. H.; Hughes, P.; Williams, K.; Leach, A. P., "Radiation-tolerant Raman distributed temperature monitoring system for large nuclear infrastructures," *IEEE Transactions on Nuclear Science,* **52**(6), 2689–2694 (2005).

[14] Bahaa E. A. Saleh, Malvin Carl Teich, [Fundamentals of Photonics], Wiley-Interscience,18-23 (2007)

[15] Xiaoguang Sun, Jie Li, Michael J. Hines, "Distributed temperature measurement using a dual-core fiber with an integrated miniature turn-around," Proc. SPIE 9852, Fiber Optic Sensors and Applications XIII, Volume 9852, id. 98520R 5 pp. (12 May 2016).

[16] A.A. Stolov, J. A. Wrubel, D. A. Simoff, Thermal stability of specialty optical fiber coatings. Observation of kinetic compensation effect, *J. Thermal Anal. Calorim.* 2016, V. 124, Issue 3, pp. 1411-1423.

[17] A. Stolov, K. Ruggles, D. Simoff, J. Li, M. Hines, An advanced polymer coating for optical fibers". SEAFOM Meeting, March 2018, Houston, TX.

[18] L. Huang, R. S. Dyer, R. J. Lago, A. A. Stolov, J. Li, Mechanical properties of polyimide coated optical fibers at elevated temperatures, Proc. SPIE, 2016, 9702, 97020Y.

[19] Matthewson, M. J., Kurkjian, C. R., Haines, C. D. and Venugopal, N., "Temperature dependence of strength and fatigue of fused silica fiber in the range 77 to 473 K," Proc. SPIE 4940, 74-79 (2003).

[20] Cusanello, V. A., Jacobson, N. J., Supczak, M. J. and Stupak, P. R., "A hermetic carbon/polyimide coating combination for adverse environments", Proc. Int. Wire & Cable Symp., 335 – 341 (1995).

[21] Lindholm, E., Li J., and Huang L., "Fiber Strength and reliability," Application Note (2015).